Denver, Colorado
NOISE-CON 2013
2013 August 26-28

Computational Aeroacoustic Modeling of Open Fan and Comparison of Predicted and Experimental Noise Fields

Sitae Kim
Yaying Niu
Yong-Joe Kim
Acoustics and Signal Process Laboratory
Mechanical Engineering Department
Texas A&M University
3123 TAMU
College Station
TX 77843-3123
joekim@tamu.edu

ABSTRACT

Modern high-speed turbo-machinery such as compressors and gas turbines can generate high level airborne noise from their fans/impellers. Here, the noise source locations and radiation characteristics of an open fan are predicted by using a Computational Aeroacoustic (CAA) model of the fan and compared to the experimental results obtained by using a Nearfield Acoustical Holography (NAH) method. The CAA model is built by using a commercial software package, ANSYS Fluent. In this model, the acoustic source data is extracted from a transient Computational Fluid Dynamic (CFD) analysis based on an unsteady k-ε turbulence model. The NAH method is applied to sound pressure data measured by using an 8×8 microphone array to visualize the three-dimensional sound pressure fields. In addition, twelve reference microphones are used to decompose twelve incoherent partial sound pressure fields from the measured data. The CAA-predicted sound fields indicate that the fan noise sources consist of a combination of monopoles at the first blade passing frequency and its higher harmonics. The CAA model can be used to predict the sound pressure fields, radiated from the open fan, which agree well with the measured results in a wide frequency span.

1. INTRODUCTION

Due to extensive applications of high-speed turbomachinery such as compressors and turbofan engines, aeroacoustic noise that is a dominant noise component of the high-speed turbo-machinery has gained significant interests. Many researchers have thus made significant efforts to identify the mechanisms of the aeroacoustic noise and suppress it by developing various analytical and numerical models, experimental techniques, and noise control strategies. Since an aeroacoustic model based on acoustic quadrupole sources induced by fluid flow stresses was firstly proposed by Lighthill[1,2], this model has been improved by other researchers during the last few decades. For example, Ffowcs Williams and Hawkings[3,4] improved the Lighthill's model by including "moving" solid boundaries, which is referred to as the Ffowcs Williams-Hawkings (FW-H) aeroacoustic analogy. Most of modern Computational Aeroacoustic (CAA) models are based on this FW-H analogy. Farassat et al.[5,6] applied the FW-H model and the Kirchhoff integral method to obtain the time-domain aeroacoustic models of rotating blades at both subsonic and supersonic blade tip speeds.

For the analysis of aeroacoustic noise generated from a high-speed turbomachinery such as a compressor, Sun et al.[7,8] developed a numerical model that can be used to calculate the fluid flow fields around a centrifugal impeller and the associated farfield aeroacoustic noise radiations. In this model, the Navier-Stokes equation along with a turbulence model was used to obtain the impeller flow fields. Then, the FW-H equation and a Boundary Element Method (BEM) were applied to the extracted dipole sources to calculate the farfield noise radiations from the dipole source distribution. Robbins et al.[9] also conducted farfield acoustic measurements to evaluate the effects of compressor inlet turbulence intensity on farfield noise radiations. All of these acoustic measurements are limited to farfields.

In the previous research conducted by the authors of this article on fan noise radiations, acoustic nearfield measurements were made with a microphone array.[10,11] By applying NAH algorithms[12-14] to the measured nearfield data, 3-D fan noise fields were reconstructed. Fan noise source locations and radiation patterns were then identified from the 3-D reconstructed noise fields. In particular, it was observed that the noise components at blade passing frequency (BPF) and its harmonics were dominant in the entire frequency span. Although the fan noise frequency components, sound source locations, and noise radiation patterns were identified from the NAH measurements, the detailed noise source distributions on fan blades are still unknown. Thus, it is critical to have a valid aeroacoustic model for analyzing open fan noise source distributions, which can lead to the optimal acoustic design of similar fans or impellers. Here, aeroacoustic modeling and predictions of the acoustic fields generated by the open axial fan are performed in this paper.

The aeroacoustic noise fields generated by the test fan are calculated by transient CFD and FW-H analogy-based CAA analyses in ANSYS Fluent. The transient CFD computations are first conducted to give aeroacoustic source data on a permeable control surface enclosing the entire test fan. Then, a FW-H analogy-based aeroacoustic model is used to calculate the acoustic pressure fields contributed by the aeroacoustic source data at the locations of the NAH array microphones. The predicted sound pressure fields are compared with experimental data for validating the CAA model. The CAA model results in the sound pressure fields, on a NAH measurement surface, showing reasonably good agreements with the measurement results. The sound source locations on a blade surface are also predicted and validated by the experimental data.

2. THEORY OF AEROACOUSTICS MODELING

The Lighthill's aeroacoustic analogy[1,2] basically introduces a quadrupole-type acoustic source term associated with turbulence stress, and thus allows the calculations of acoustic source data in a predefined control volume inside a CFD computation domain. The Lighthill's equation can be obtained from the Mass and Momentum Conservation Equations by considering the density perturbation with respect to the ambient condition: i.e., $\rho' = \rho - \rho_0$. In form of an inhomogeneous wave equation, the Lighthill's equation is then written as

$$\frac{\partial^2 \rho'}{\partial t^2} - c^2 \nabla^2 \rho' = \frac{\partial^2 T_{ij}}{\partial x_i \partial x_j} \tag{1}$$

where c is the speed of sound and T_{ij} is the Lighthill stress tensor defined as

$$T_{ij} = \rho v_i v_j + \sigma_{ij} - c^2 \rho' \delta_{ij} \tag{2}$$

The Lighthill's aeroacoustic analogy describes free-field sound generated by the turbulence stress of fluid flow without foreign bodies submerged in a fluid medium. The solution to the Lighthill's equation is obtained by using a free-space Green's function: i.e.,

$$\rho'(\mathbf{x},t) = \frac{1}{4\pi c^2}\frac{\partial^2}{\partial x_i \partial x_j}\int_V \frac{T_{ij}(\mathbf{y}, t-|\mathbf{x}-\mathbf{y}|/c)}{|\mathbf{x}-\mathbf{y}|}d^3\mathbf{y} \tag{3}$$

where **x** and **y** are the vectors pointing receiver and source coordinates, respectively. Time t is defined at the receiver location and $\tau = (t - |\mathbf{x} - \mathbf{y}|/c)$ represents the time, at the source location, which is referred to as the retarded time.

When a system of interest includes an arbitrarily moving solid body submerged in a fluid medium, the Ffowcs Williams-Hawkings (FW-H) aeroacoustic analogy[3,4] is the most commonly-used for the aeroacoustic analysis of this system. The solution to the FW-H equation is obtained by using a free-space Green's function: i.e.,

$$4\pi p(\mathbf{x},t) = \frac{\partial^2}{\partial x_i \partial x_j}\int_V \frac{T_{ij}}{r|1-M_r|}d^3\mathbf{y} - \frac{\partial}{\partial x_i}\int_s \frac{\rho v_i (v_i - u_j) + \sigma_{ij}}{r|1-M_r|}n_j d^2\mathbf{y} + \frac{\partial}{\partial t}\int_s \frac{\rho(v_i - u_j) + \rho_0 u_i}{r|1-M_r|}n_i d^2\mathbf{y} \tag{4}$$

where n_i is the unit normal vector to the source surface, M_r is the Mach number of the source surface velocity component along the direction of the radiation vector, **r**: i.e., $M_r = M_i r_i$. In Eq. (4), the first surface integral, that is a quadrupole-type, represents the sound source due to the turbulence stress inside the permeable source surface and the second and third surface integrals of dipole- and monopole-types represent the force from the control surface to the fluid medium and the mass flow through the permeable surface, respectively. In the current aeroacoustic analyses, the source surface is defined on the outer permeable surface of a control volume enclosing the fan blades. Therefore, the acoustic source consists of all the aforementioned source types. The acoustic pressures at predefined receiver locations are thus evaluated by Eq. (4) once the source data (i.e., fluid flow velocities and pressures) are obtained from transient CFD computations.

3. PROCEDURES OF CFD AND CAA ANALYSES

In order to perform CAA predictions, transient CFD calculations are required prior to calculate acoustic source terms on a source surface as in Eq. (4). The modeling of the test fan and the meshing of a computation domain are thus first completed by using SolidWorks and ANSYS Gambit. Then, the discretized model is imported into ANSYS Fluent for transient CFD and CAA analyses.

A. Modeling of fluid volumes surrounding the test fan

The open fan model is built by using commercial software packages such as SolidWorks and ANSYS Gambit. The fluid zones are obtained by creating volumes enclosing the solid fan model and performing Boolean subtractions. As shown in Fig. 1, the outer surface of the cylindrical volume is chosen as a permeable control surface (i.e., acoustic source surface) and the cylindrical volume is thus an acoustic control volume including quadrupole-type sound sources induced by turbulent flows. The cylindrical control volume is placed in a large brick volume that simulates free-field conditions. The brick volume has the height of 1.5 m and both the depth and width of 0.8 m. These two fluid volumes are separated by the interfaces coincident with the control surface.

B. Meshing of fluid volumes

Before meshing the fluid volumes, boundary layer meshes and fan blade face meshes are generated in Gambit. Then, unstructured "tetra" volume meshes for the cylindrical control volume are generated by defining a size function with the mesh growth rate of 1.2 relative to the boundary layer meshes and the maximum mesh size of 5 mm. The volume meshes for the outer fluid zone are generated by non-conformally attaching the first layer of meshes to the cylindrical control volume and defining the size function with the growth rate of 1.2 and the maximum mesh size of 25 mm: see Fig. 1 for the final volume meshes of the two fluid zones. The total number of the volume meshes is approximately 3.6 million. This fluid volume model is then imported into Fluent for the CFD and CAA analyses.

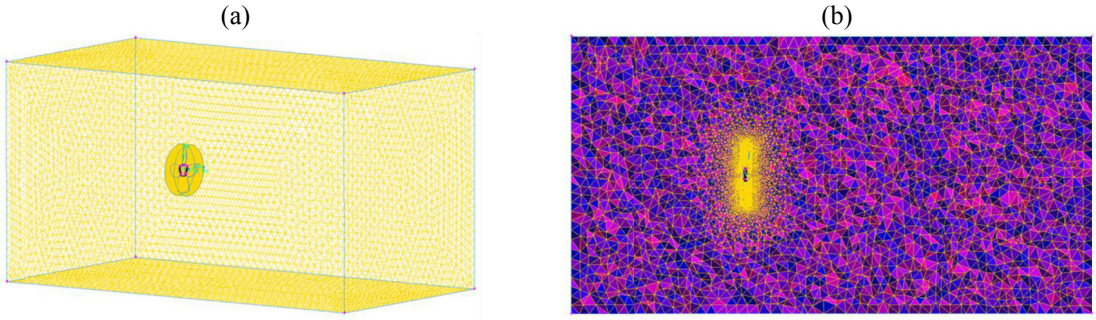

Figure 1: Meshes of cylindrical and brick fluid volumes:

(a) Volume meshes with 3.6 million elements and **(b)** Cross-sectional view of volume meshes.

C. CFD and CAA simulation process

The transient CFD computations are conducted prior to extract temporal acoustic source data as shown in Eq. (4). For the unsteady transient computations, the cylindrical control volume is defined as a "moving mesh" with the sliding interfaces defined on the control surface. The test fan speeds are set to 4.3 and 5.1 kRPM for the current CFD analyses.

The acoustic source data are saved at each time step during the transient CFD computations. The total record length for the acoustic source data is 0.2 second, i.e., 2000 time steps with the sampling interval of 0.0001 second. The saved acoustic source data are then used to compute acoustic pressure fields using the FW-H aeroacoustic model at the given receiver locations. In the current research, the source surface defined on the permeable control surface can also include the broadband turbulent flow noise components. The receivers are defined at the same locations of the array microphones shown in Fig. 2.

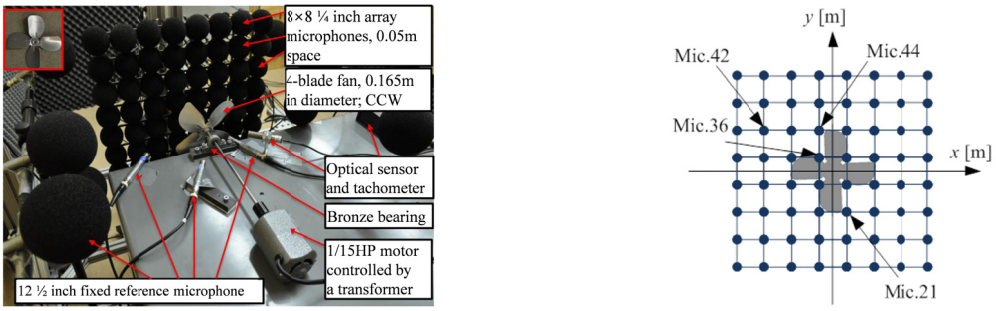

Figure 2: Fan noise experimental setup and selected array microphones.

4. NUMERICAL AND EXPERIMENTAL RESULTS

In the transient CFD analysis, the predicted velocity vectors, vorticity magnitudes, and turbulence intensities are analyzed on a blade surface at the fan speed of 4.3 and 5.1 kRPM (see Figs. 3(a) to 3(f)). From this information, the detailed noise source distributions on fan blades can be identified, which could not be obtained from the NAH measurements in Ref. 10. All of the CFD calculated fields indicate that the maximum magnitude of velocity vectors, vorticity, turbulence intensities lay on the blade surface tips. Therefore, it can be deduced that the blade tips could radiate significant aeroacoustic noise compared to other blade locations.

At the location of microphone 21 as indicated in Fig. 2, Fig. 4(a) shows the comparison between the CAA predicted sound pressure spectrum (in red dotted line) and the directly measured sound pressure spectrum (i.e., the total sound pressure spectrum before decomposed into multiple partial fields in blue dash line) at the fan speed of 4.3 kRPM. Figure 4(b) shows the comparison of the CAA predicted sound pressure spectrum and the first partial field of the measured sound pressure spectrum at the same fan speed. Figure 4(a) shows that the CAA predicted sound pressure matches well with the "directly" measured sound pressure spectrum for broadband turbulent flow noise components (e.g., above 1500 Hz), while Fig. 4(b) indicates that the CAA prediction result agrees well with the first partial field of the measured data for low frequency components (e.g., below 500 Hz). For the BPF components, both the first partial field and directly measured spectra agree well with the CAA predicted spectrum: e.g., see the 1st BPF components at 288 Hz in Figs. 4(a) and 4(b). Note that the fluctuations of the CAA predicted sound pressures, e.g., at the high frequencies above 1500 Hz are caused by the relatively small number of averages (i.e., 7 averages with 2000 time data points and 75% overlapping) when calculating the predicted spectral results. These fluctuations are associated with random turbulence noise and can be reduced by increasing the number of averages, although the computation time increases accordingly. Although there is the random turbulence noise, the CAA prediction still matches with the directly measured sound pressure spectrum reasonably well at the high frequencies as shown in Fig. 4(a).

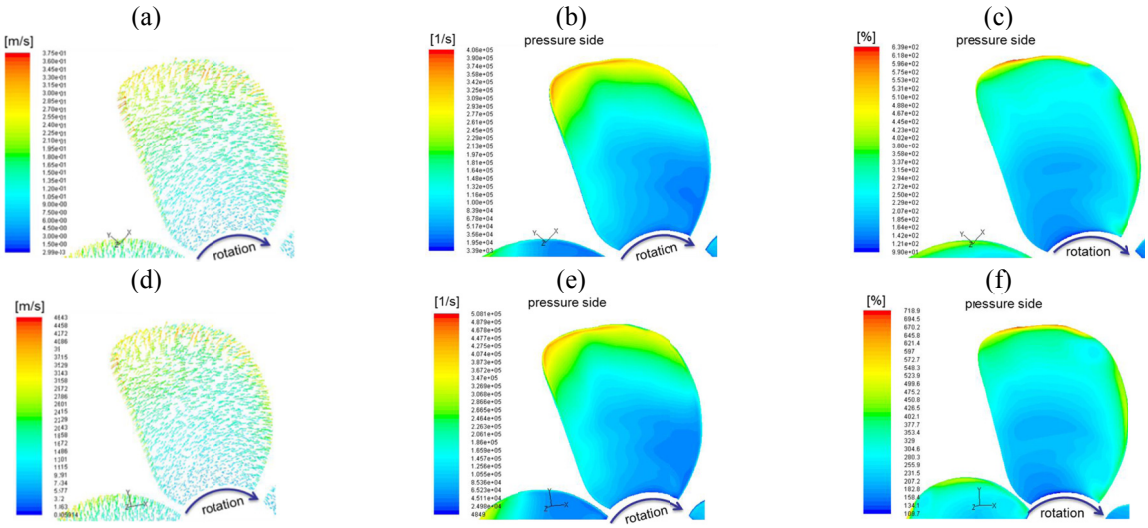

Figure 3: CAA predicted noise sources distributions on a blade pressure side: **(a)** Fluid velocity vectors at 4.3 kRPM(72Hz), **(b)** Vorticity magnitudes at 4.3 kRPM(72Hz), **(c)** Turbulence intensity at 4.3 kRPM(72Hz), **(d)** Fluid velocity vectors at 5.1 kRPM(86Hz), **(e)** Vorticity magnitudes at 5.1 kRPM(86Hz), **(f)** Turbulence intensity at 5.1 kRPM(86Hz)

Figures 4(c) to 4(h) present the similar comparisons shown in Figs. 4(a) and 4(b), with the other three microphones. The 1st BPF components are well predicted at the all selected microphone locations. The low frequency components are predicted reasonably well when compared with the first partial sound pressure fields. The broadband turbulence noise components at the high frequencies are also predicted correctly although there are the random turbulence noise errors. At some microphone locations, e.g., microphones 36, 42, and 44, the second BPF components show, in particular, good agreements between the measured and predicted results.

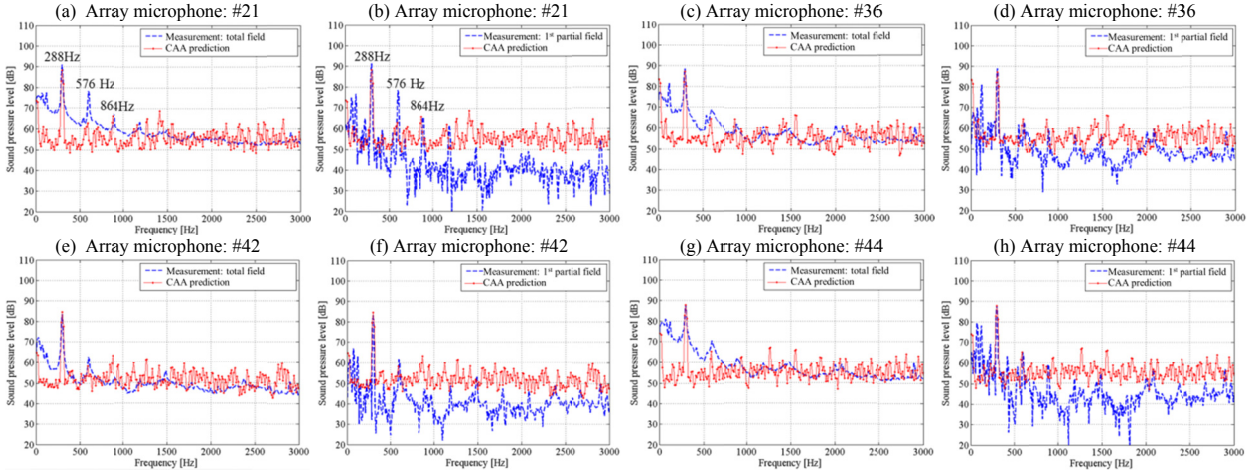

Figure 4: Measured and CAA predicted sound pressure spectra at 4.3 kRPM (72 Hz): **(a)** Directly measured sound pressure spectrum (i.e., total sound pressure field) and CAA prediction at microphone 21, **(b)** First partial field of measured sound pressure and CAA prediction at microphone 21, **(c)** Total field and CAA prediction at microphone 36, **(d)** First partial field and CAA prediction at microphone 36, **(e)** Total field and CAA prediction at microphone 42, **(f)** First partial field and CAA prediction at microphone 42, **(g)** Total field and CAA prediction at microphone 44, and **(h)** First partial field and CAA prediction at microphone 44.

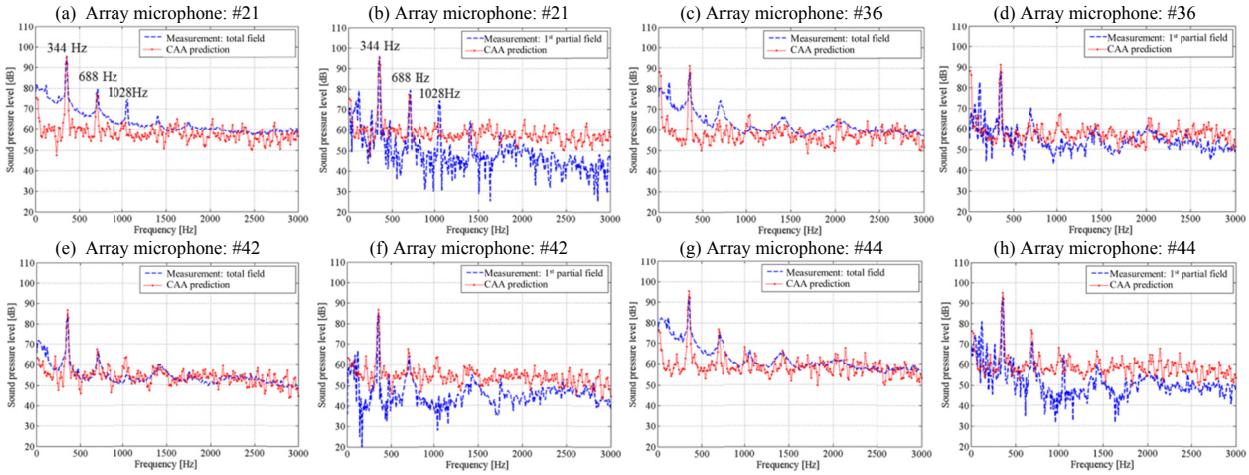

Figure 5: Measured and CAA predicted sound pressure spectra at 5.1 kRPM (86 Hz): **(a)** Directly measured sound pressure spectrum (i.e., total field) and CAA prediction at microphone 21, **(b)** First partial field of measured sound pressure and CAA prediction at microphone 21, **(c)** Total field and CAA prediction at microphone 36, **(d)** First partial field and CAA prediction at microphone 36, **(e)** Total field and CAA prediction at microphone 42, **(f)** First partial field and CAA prediction at microphone 42, **(g)** Total field and CAA prediction at microphone 44, and **(h)** First partial field and CAA prediction at microphone 44.

At the fan speed of 5.1 kRPM, Figs. 5(a) to 5(h) show that the CAA-predicted results agree well with the measured results at the 4 microphone locations as described in Fig. 2. The low frequency, 1st and 2nd BPFs, and broadband turbulence noise components are all predicted correctly. The sound pressures in Fig. 5 at 5.1 kRPM have the higher sound pressure amplitudes than those at 4.3 kRPM due to increased vorticity and turbulence intensity magnitudes.

Since the 1st BPF components have the most dominant amplitudes at the all microphone locations, the measured and predicted sound pressure fields at the 1st BPFs of 288 Hz and 344 Hz are plotted on the measurement surface in Figs. 6 and 7 for the fan speed cases of 4.3 and 5.1 kRPM, respectively. Both the measured and CAA predicted sound pressure fields show significant noise radiations from blade tips (see Figs. 6(a), 6(b), 7(a), and 7(b)). The CAA predicted sound pressure fields match well with the measurement results, particularly, at the blade tip locations. The prediction errors in Figs. 6(c) and 7(c) verify the good agreements between the measurements and predictions on the measurement surface, except at a few locations close to the edges of the plots. In the previous article[10] on NAH measurements, it is shown that the noise radiations can be modeled by combining monopoles placed at the blade tips.

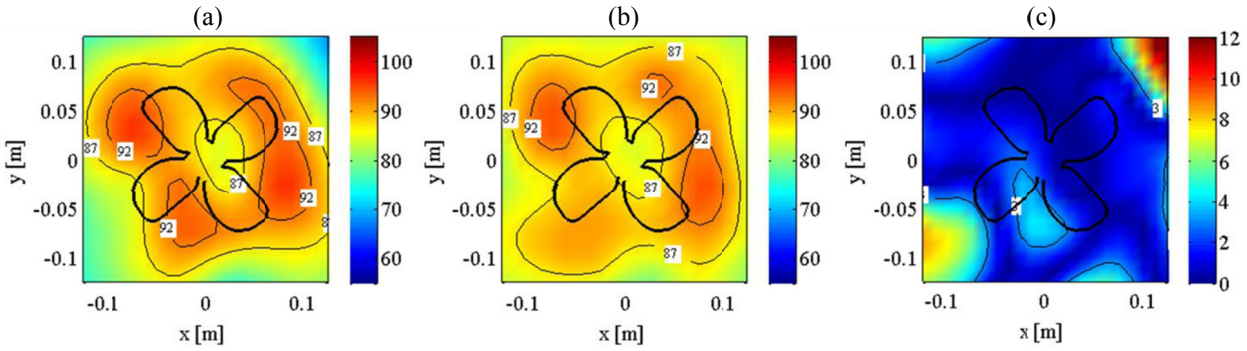

Figure 6: Sound pressure fields on measurement surface at 1st BPF of 288Hz (4.3kRPM, 72Hz) [dB]: **(a)** 1st partial field of measured sound pressure, **(b)** CAA predicted sound pressure, and **(c)** prediction error.

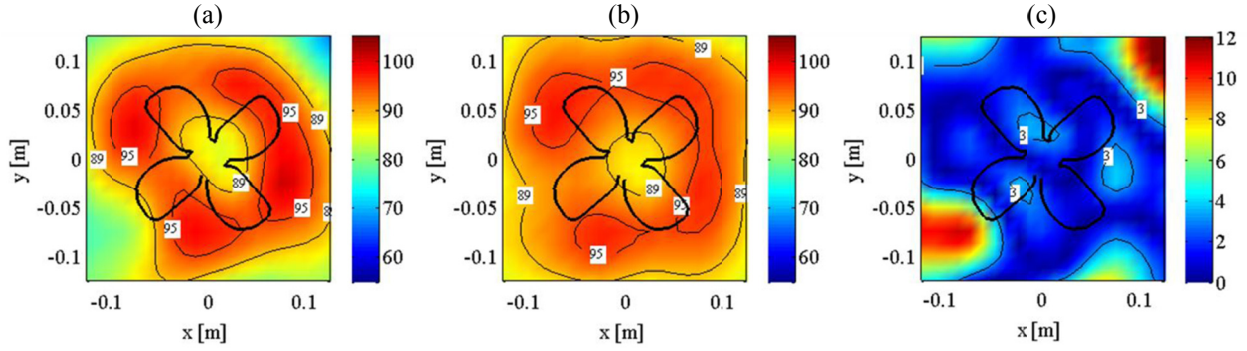

Figure 7: Sound pressure fields on measurement surface at 1st BPF of 344Hz (5.1kRPM, 86Hz) [dB]: **(a)** 1st partial field of measured sound pressure, **(b)** CAA predicted sound pressure, and **(c)** prediction error.

5. CONCLUSIONS

In this research, the CFD and CAA analyses were performed to predict the sound pressure fields generated by the test fan at the speeds of 4.3 and 5.1 kRPM and the predicted sound pressure fields are then compared with the experimental results.

The 3-D fluid volume model enclosing the test fan is first created in ANSYS Gambit, and the unstructured "tetra" volume meshes are generated for the CFD and CAA analyses in ANSYS Fluent. Based on the FW-H aeroacoustic analogy, the solid fan is enclosed by a cylindrical permeable control surface that is placed in the large volume simulating free-field conditions. The permeable control surface is used as the acoustic source surface on which sound source data are saved from the transient CFD computations. The saved acoustic source data are then used to calculate the sound pressures at the given microphone positions.

The first partial fields of the measured sound pressure spectra show good agreements with the predicted ones at the BPFs and low frequencies, while the directly measured sound pressure spectra show acceptable agreements at the BPFs and high frequencies. At the first BPFs of the two fan speeds, the CAA predicted sound pressure fields match well with the measured ones on the measurement surface, particularly, at the blade tip locations. Therefore, it is concluded that the FW-H analogy-based aeroacoustic model can be used to successfully predict the sound pressure fields generated by the open axial fan.

ACKNOWLEDGEMENTS

This work was sponsored by the Turbomachinery Research Consortium of Texas A&M University.

REFERENCES

1. M. J. Lighthill, "On sound generated aerodynamically: I. General theory," *Proc. R. Soc. Series A*, **211**, 564 – 587(1952).
2. M. J. Lighthill, "On sound generated aerodynamically: II. Turbulence as a source of sound," *Proc. R. Soc. Series A*, **222**, 1 – 32(1954).
3. J. E. Ffowcs Williams and D. L. Hawkings, "Sound generation by turbulence and surfaces in arbitrary motion," *Phil. Trans. R. Soc. Series A*, **264**(1151), 321 – 342 (1969).
4. A. P. Dowling and J. E. Ffowcs Williams, *Sound and Sources of Sound*, (Wiley, New York, 1983).
5. F. Farassat and M. K. Myers, "Extension of Kirchhoff's formula to radiation from moving surfaces," *J. Sound Vib.*, **123**(3), 451 – 460 (1988).
6. F. Farassat, "Acoustic radiation from rotating blades – the Kirchhoff method in aeroacoustics," *J. Sound Vib.*, **239**(4), 785 – 800 (2001).
7. H. Sun and S. Lee, "Letter to the editor: Numerical prediction of centrifugal compressor noise," *J. Sound Vib.*, **269**, 421 – 430 (2004).
8. H. Sun, H. Shin, and S. Lee, "Analysis and optimization of aerodynamic noise in a centrifugal compressor," *J. Sound Vib*., **289**, 999 – 1018 (2006).
9. B. Robbins and B. Lakshminarayana, "Effect of inlet turbulence on compressor noise," *J. Aircraft*, **11**(5), 273 – 281 (1974).
10. Y. Niu and and Y.-J. Kim. "Three-dimensional visualizations of open fan noise fields," *Noise Control Eng. J.* **60(4)**, 392-404 (2012)
11. Y. Niu and and Y.-J. Kim. "Study on turbomachinery fan and impeller noise sources and their vibro-acoustic coupling effects on possible structural failure," Research Report to Turbomachinery Research Consortium at Texas A&M University, Report #**TRC-B&C-10-12** (2012)
12. H.-S. Kwon, Y.-J. Kim, and J. S. Bolton, "Compensation for source nonstationarity in multireference, scan-based near-field acoustical holography," *J. Acoust. Soc. Am.*, **113**, 360 – 368 (2003).
13. H.-S. Kwon, Y. Niu, and Y.-J. Kim, "Planar nearfield acoustical holography in moving fluid medium at subsonic and uniform velocity," *J. Acoust. Soc. Am*., **128** (4), 1823 – 1832 (2010).
14. Y.-J. Kim and Y. Niu, "Improved statistically optimal nearfield acoustical holography in subsonically moving fluid medium," *J. Sound Vib.*, 3945-3960 (2012).